Nature and origin of white efflorescence on bricks, artificial stones and joint mortars of modern houses evaluated by portable Raman spectroscopy and laboratory analyses

Héctor Morillas, Maite Maguregui, Josu Trebolazabala, Juan Manuel Madariaga

PII: S1386-1425(14)01502-9
DOI: http://dx.doi.org/10.1016/j.saa.2014.10.006
Reference: SAA 12820

To appear in: *Spectrochimica Acta Part A: Molecular and Biomolecular Spectroscopy*

Received Date: 18 February 2014
Revised Date: 9 June 2014
Accepted Date: 6 October 2014

Please cite this article as: H. Morillas, M. Maguregui, J. Trebolazabala, J.M. Madariaga, Nature and origin of white efflorescence on bricks, artificial stones and joint mortars of modern houses evaluated by portable Raman spectroscopy and laboratory analyses, *Spectrochimica Acta Part A: Molecular and Biomolecular Spectroscopy* (2015) Volume 136, Part B, 5 February 2015, Pages 1195-1203, doi: http://dx.doi.org/10.1016/j.saa.2014.10.006

Nature and origin of white efflorescence on bricks, artificial stones, and joint mortars of modern houses evaluated by portable Raman spectroscopy and laboratory analyses

Héctor Morillas[1]*, Maite Maguregui[2], Josu Trebolazabala[2] and Juan Manuel Madariaga[1]

[1]Department of Analytical Chemistry, Faculty of Science and Technology, University of the Basque Country UPV/EHU, P.O. Box 644, 48080 Bilbao, Basque Country, Spain;
* Corresponding Author: Tel: +34 946018298; Fax: +34 946013500 e-mail: hector.morillas@ehu.es
[2]Department of Analytical Chemistry, Faculty of Pharmacy, University of the Basque Country UPV/EHU, P.O. Box 450, 01080 Vitoria-Gasteiz, Basque Country, Spain

ABSTRACT

Bricks and mortar currently constitute one of the most important building materials used in the construction of most modern facades. The deterioration of these materials is caused primarily by the impact of numerous external stressors, while poor manufacturing quality, particularly of mortars, can also contribute to this process. In this work, the non-invasive Raman spectroscopy technique was used to identify the recently formed deterioration compounds (primarily sulfates and nitrates) in bricks, artificial stones, and joint mortars from detached houses in the Bilbao metropolitan area (Basque Country, North of Spain), as well as to investigate the deterioration processes taking place in these materials. Additionally, to confirm and in some cases complement the results obtained with Raman spectroscopy, SEM-EDS and XRD measurements were also carried out.

KEYWORDS: Portable Raman spectroscopy, brick, mortar, sulfates, nitrates.

INTRODUCTION

Bricks and stones are two of the most durable building materials, which in most cases can be preserved for years and generally do not require any maintenance [1]. Owing to the industrial development in the nineteenth century, the use of bricks attained great importance and became a standard in the construction of homes. The durability of well-manufactured brick is comparable to that of stone-based materials, while the former has the advantage of being more easily shaped.

Mortar, a mixture of inorganic binders, sand, and water, has been in use since the time of the ancient Egyptians. Depending on the type of mortar and the components being joined, different additives can be used in the mixture [2].

Artificial stone is another material commonly used in construction, the generalized use of which dates from the nineteenth century. It consists primarily of a mixture of modern (usually a Portland type) cement, siliceous sand, gravel, and water. Depending on the proportion of each component in the mixture, the artificial stone can be produced with properties such as porosity, capillarity, and level of thermal insulation that differ from those of natural stones [3, 4].

Although there are buildings that over hundreds of years have nearly maintained their original aesthetic and mechanical features, there are several examples of impacts on the walls (both inside and outside) of such historical constructions [5-8], caused primarily by modern urban-industrial environments. Moreover, such environments particularly affect recently built facades, with significant degradations showing after only a few decades [9]. To slow down such degradations, new processes based on the use of coating materials have been proposed in recent years [10].

Building facades suffer from various degrees of exposure to heat, humidity, atmospheric acidic gases, and wind pressure as well from infiltration by aqueous solutions.

Considering these sources of deterioration, several examples of building material degradation are commonly observed:

- Brick walls exhibiting soil and green plant growth from the ground level until a given height.
- The detachment of bricks above windows when the joint mortar reaches a high proportion of white efflorescence crystals.
- Planters enclosed in the facade exhibiting efflorescence after a few years of watering.
- The accumulation of white salts on facades when the surface is wetted with a salt solution (wind most likely moves ions dissolved in rainwater and the salts precipitate when the surface is wetted).
- The vertical displacement of white efflorescence caused by green grass on the street level.

In all of these cases, infiltration water carrying dissolved ions is the primary cause of the crystallization of salts. This takes place when the infiltration water reaches supersaturation and the thermodynamic characteristics of the media are adequate for the formation of a crystal nucleus. The crystallizations can occur at the surface (efflorescence) or within the porous structure of the building materials (subefflorescence). The impact of water infiltration (both crystallization and the dissolving of salts as a consequence of rainwater) over an extended period of time can contribute to the disintegration of building material [11]. On the other hand, mineralogical and chemical changes originating from salt mineralizations can induce structural changes by promoting cracks and disintegration [12] in joint mortar, bricks, and even artificial stones. Recently, laboratory simulations and accelerated weathering experiments that reproduce environmental attacks on samples of historical bricks have been carried out to establish the nature and formation mechanisms of such efflorescences [13].

Numerous studies can be found in the literature that span a wide range of useful analytical techniques used to identify the damage promoted by efflorescence and the soluble salts present in building materials [14, 15]. Techniques such as optical microscopy, X-ray diffraction, electron scanning microscopy, and thermogravimetric

analysis [16, 17] have been used to characterize the efflorescences as well as the chemical and mineralogical changes in building materials. Infrared and Raman spectroscopy can also now be used as an alternative analytical technique for this purpose [18], especially since the development of portable instrumentation to perform analyses in the field [19, 20].

In this work, a simple and non-destructive Raman spectrometer was used to perform a field analysis in which both the original and deterioration compounds present in facades from recently erected houses located in the metropolitan area of Bilbao (Basque Country, North of Spain) were characterized. To confirm and complement these in situ measurements, additional analyses were conducted in the laboratory using a benchtop Raman spectrometer as well as the SEM-EDS and XRD techniques. The primary materials used in the facades of the selected houses include bricks, artificial stones, and joint mortars. The facades were neither painted nor had a protection layer against rain or infiltration water.

MATERIAL AND METHODS

Description of the samples and locations

The studied facades were from houses built in 2002 and located in a residential zone of the Metropolitan area of Bilbao (Basque Country, Northern Spain, see Fig. 1A). All of these homes have two floors, a terrace, and a garden. The primary materials used in the construction of their facades are bricks, artificial stones, and their respective joint mortars. A previous screening from different houses in the same residential area was performed using a portable Raman spectrometer. Three facades from the areas most by impacted by environmentally driven deterioration were selected to perform the study:

- House 1 has a southwest-oriented facade of exposed brick connected with joint mortar. This facade has direct contact with the green grass of the garden but is protected from the main winds and rainfall.
- House 2 has a southwest-oriented facade built from artificial stones supporting the garden, the soil of which meets the facade at the rear side of the home. The

analyzed portion is protected from the main winds and rainfall, although the garden at the back of the home is exposed to the latter.

- House 3 has a northwest-oriented facade composed of exposed brick connected with joint mortar. The orientation of this facade exposes it to both the main winds and rainfall.

A schematic representation of the building pathologies identified in each of these detached houses can be viewed in Fig. 1B. White efflorescence samples as well as some detached brick, artificial stone, and joint mortar samples were collected from the areas showing different Raman features during similar climatic conditions (absence of rain for 15 days, low temperature between 2ºC and 5ºC) in December 2012 and January 2013. The samples taken never exceeded 2 x 2 cm in size.

Instrumentation

Two Raman spectrometers were employed for the characterization of the samples: a portable spectrometer for the in situ or field analysis in which samples are screened without being removed and a benchtop spectrometer for an in-depth study to identify the maximum number of compounds in each sample. The portable innoRam™ ($B_{\&}WTEK_{INC.}$, Newark, USA) Raman spectrometer utilizes a 785 nm excitation laser and has a maximum output power of 300 mW. Variable attenuation of the output power was achieved through the implementation of filters, which allowed for the reduction of the output power down to 1% of the maximum. The spectra were typically collected using a wavelength range of 100 to 2200 cm^{-1}, although in some measurements larger ranges were used. The exposure time for each spectrum ranged from 2 to 10 s, and two to fifteen repeated acquisitions were averaged to improve the signal-to-noise ratio. The Raman microprobe (approximately 0.1 mm focal spot size) can be operated by hand or mounted on a manual X-Y-Z manipulator with a micro video camera to assist in the alignment (MICROBEAM S.A, Barcelona, Spain).

The laboratory-based measurements were carried out using a Renishaw RA100 Raman microprobe (Renishaw, Gloucestershire, UK), which also utilizes a 785 nm excitation laser. The microscopic analysis was performed using 20x and 50x long-range objective lenses mounted in the head of the Raman microprobe, which also has a micro-video camera. The spectra were typically collected from 100 to 3000 cm^{-1}, although larger wavelength ranges were also employed in some of the measurements. The exposure

time for each spectrum ranged from 2 to 10 s, and ten to fifty repeated acquisitions were averaged to increase the signal-to-noise ratio.

For both measurements, the laser power was attenuated to avoid thermal decomposition of the sample. Both Raman instruments were calibrated daily using the 520 cm^{-1} Raman band of a crystalline silicon chip. Spectral acquisition with the innoRam™ and RA100 spectrometers was performed using the BWSpec™ 3.26 software package ($B\&WTEK_{INC.}$) and the Renishaw Wire 3.2 software package, respectively. The Raman data were interpreted by comparing the acquired spectra with the spectra of pure standard compounds obtained from the e-VISNICH dispersive Raman database, which contains Raman spectra of Natural, Industrial and Cultural Heritage compounds, following a methodology described elsewhere [21]. Open access Raman spectral databases (e.g., RRUFF [22]) were also used in assigning some of the Raman bands. The spectral interpretation and data treatment were carried out using the GRAMS/AI 7.02 software package (Thermo Fisher Scientific Inc., Waltham, USA).

To corroborate some of the results, X-ray diffraction analyses were performed with a PANalytical Xpert PRO powder diffractometer equipped with a copper tube ($\lambda_{CuK\alpha media}$= 1.5418 Å, $\lambda_{CuK\alpha1}$= 1.54060 Å, $\lambda_{CuK\alpha2}$= 1.54439 Å), vertical goniometer (Bragg-Brentano geometry), programmable divergence aperture, automatic sample changer, secondary graphite monochromator, and PixCel detector. The operating conditions for the Cu tube were 40 kV and 40 mA, and the angular range (2θ) was scanned between 5 and 70°. The treatment of the diffractogram data and the identification of the mineral phases present was carried out with the X'pert HighScore (PANalytical) software package in combination with the Powder Diffraction File (PDF-2) database (International Centre for Diffraction Data - ICDD, Pennsylvania, USA).

For the acquisition of electron images and the determination of elemental compositions in the samples, SEM-EDS analyses were carried out using an EVO®40 Scanning Electron Microscope (Carl Zeiss NTS GmbH, Germany) coupled to an X-Max Energy-Dispersive X-ray spectroscopy system (Oxford Instruments, Abingdon, Oxfordshire, United Kingdom). The SEM images were obtained under high vacuum using an acceleration voltage of 20 kV and a working distance of 6–13 mm. The images were collected using a secondary electron detector at different magnifications (up to

10,000x). The elemental analysis was carried out using an 8.5 mm working distance, a 35 ° take-off angle, and an acceleration voltage of 20 KV. An integration time of 50 s was employed to achieve a good signal to noise ratio.

RESULTS AND DISCUSSION

House 1

The Raman analyses were conducted for two types of building materials used in this house. First, efflorescent samples present on bricks and the surface of the joint mortars of artificial stones were analyzed. The Raman spectra obtained from efflorescence on brick exhibited a band at 1049 cm^{-1} (see Fig. 2A). The band at 1049 cm^{-1} can be assigned to the ν_1 symmetric stretching mode of the NO_3^- group of niter (KNO_3) or nitrocalcite ($Ca(NO_3)_2 \cdot 4H_2O$) [20,23]. In certain Raman spectra, in addition to the bands at 1049 and 985 cm^{-1}, bands at 715, 1344, and 1358 cm^{-1} were also identified (see Figure 2A). The presence of these bands confirms that niter is the main nitrate salt crystallized in these samples. In addition to the nitrate Raman bands, a band at 985 cm^{-1} corresponding to the ν_1 symmetric stretching mode of the SO_4^{2-} group in epsomite ($MgSO_4 \cdot 7H_2O$), was also identified in these efflorescences (see Fig. 2A). Epsomite has been identified in efflorescences on bricks in previous studies [24]. Furthermore, in several spectra acquired from the same efflorescences, a band at 992 cm^{-1} originating from thenardite (Na_2SO_4) was also identified, as discussed below.

The Raman analyses performed on efflorescences from the joint mortars revealed three main compounds, present either mixed together or alone. The in situ spectra displayed only the main bands of thenardite and niter at 992 and 1049 cm^{-1}, respectively. The main band at 992 cm^{-1} corresponds to the ν_1 symmetric stretching mode of the SO_4^{2-} group in thenardite.

In the laboratory analyses, in addition to the main band of thenardite, bands originating from the sulfate group were also observed at 403, 450, 620, 632, 645, 992, 1101, 1130, and 1152 cm^{-1}. Moreover, the ν_4 anti-symmetric bending (715 cm^{-1}), ν_1 symmetric stretching (1049 cm^{-1}), and ν_3 anti-symmetric stretching modes (1344 and 1358 cm^{-1}) of the NO_3^- group of niter were also observed, together with the ν_4 anti-symmetric bending

(724 cm^{-1}) and ν_1 symmetric stretching (1067 cm^{-1}) modes of the NO_3^- group of nitratine ($NaNO_3$) (see Fig. 2B). Sodium nitrate has also been identified by Raman spectroscopy in previous studies on carbonate substrate-based mortars, [25]. Sodium nitrate can appear as a deterioration product originating from trona ($Na_3(HCO_3)(CO_3)\cdot 2H_2O$), which can be present in the substrate material. Trona can be formed in the mortar setting, and upon air exposure this mixed carbonate-bicarbonate can be attacked by ammonium nitrate (most likely originating from nitrate salts transported by infiltration waters), leading to the formation of sodium nitrate through the following reaction:

$$3\ NH_4NO_3 + Na_3(HCO_3)(CO_3)\cdot 2H_2O \rightarrow 3\ NaNO_3 + 2\ HCO_3^- + NH_3\ (g) + 2\ NH_4^+ \quad (1)$$

In the Raman analysis performed on small dots resembling efflorescence located in the holes of the joint mortar samples, the main bands of thenardite and niter as well as a band at 1062 cm^{-1} belonging to trona were observed (see Fig. 2C). The identification of trona in the joint mortar reinforces the hypothesis discussed above regarding nitratine formation. Additionally, peaks corresponding to the ν_1 symmetric stretching mode of the CO_3^{2-} group of calcite ($CaCO_3$) at 1086 cm^{-1} and the ν_1 symmetric stretching mode of the CO_3^{2-} group of dolomite ($MgCa(CO_3)_2$) at 1095 cm^{-1} [26] were observed. Moreover, the signal-to-noise ratio of the spectra was high enough to allow secondary bands of these major compounds to be observed (see Fig. 2C). In addition to the deterioration compounds located in the bulk of the joint mortars, the bending vibrations of the intra-tetrahedral O-Si-O angles from quartz (SiO_2) located at 465 cm^{-1} and the anti-symmetric stretching mode of the MnO_6 octaedra in pyrolusite (MnO_2) at 647 cm^{-1} were also identified (see Fig. 2D). The presence of pyrolusite in the joint mortars was also confirmed via SEM-EDS and XRD analyses (see Figs. 3A and 3B). Some groups have also previously reported the presence of pyrolusite in mortars [27]. A band at 936 cm^{-1} that can be assigned to the ν_1 symmetric stretching mode of the PO_4^{3-} group of anapaite ($Ca_2Fe_2(PO_4)_2\cdot 4H_2O$) (see Fig. 3B) was also identified in the Raman measurements of the joint mortars. The presence of anapaite in the joint mortar was also confirmed via SEM-EDS and XRD (see Figs. 3A and 3B). Although there is no mention of the use of anapaite as additive in the literature, it is well known that phosphates are commonly used to retard the setting of concrete [28, 29].

House 2

Several whitish patinas were identified on the artificial stones of the facade from House 2 (see Fig. 4). To the best of our knowledge, there are no literature reports on the analysis of this type of material using Raman spectroscopy. In this work, the whitish patinas were characterized in situ as well as analyzed in the laboratory using the previously mentioned techniques. The Raman spectra of these patinas exhibited a band at 992 cm^{-1} belonging to the deterioration compound thenardite. Moreover, a band was identified at 647 cm^{-1} as corresponding to pyrolusite, which is present in the original material. Additionally, in some of the Raman spectra, bands at 578 and 643 cm^{-1} assignable to birnessite-type manganese oxides were also observed [30]. XRD measurements confirmed the presence of pyrolusite as well as that of calcite, quartz, and gypsum ($CaSO_4 \cdot 2H_2O$) (see Fig. 3D).

Additional sulfate compounds were clearly identified in the efflorescences from the whitish patina. For example, the spectrum in Fig. 4A displays bands at 980, 1008, 1025, and 1086 cm^{-1} that correspond to the ν_1 symmetric stretching mode of the SO_4^{2-} group of syngenite ($K_2Ca(SO_4) \cdot H_2O$) and gypsum ($CaSO_4 \cdot 2H_2O$), to the ν_3 asymmetric stretching mode of the SO_4^{2-} group of (para)coquimbite ($Fe_2(SO_4)_3 \cdot 9H_2O$), and to the ν_1 symmetric stretching mode of the CO_3^{2-} group of calcium carbonate, respectively. In addition, a band at 280 cm^{-1} that can be assigned to calcite or aragonite is also present in the same spectrum (Fig. 4A). Moreover, the appearance of another band at 711 cm^{-1} suggests that calcite is the main polymorph of calcium carbonate present in the sample.

The Raman identification of (para)coquimbite was carried out based on the presence of its main band at 1025 cm^{-1}; however, it is difficult to affirm whether coquimbite, paracoquimbite polymorph, or a mixture of both is present in the sample on the basis of only this main band. (Para)coquimbite can be formed in these samples as a consequence of a sulfation process involving iron (III) oxides and oxyhidroxides [31]. Both iron oxyhidroxides (e.g., limonite ($Fe_2O_4 \cdot H_2O$) with main bands at 298 and 392 cm^{-1}) and iron (III) oxides (e.g., hematite (Fe_2O_3) with main bands at 225, 291, and 405 cm^{-1}) were

identified in the sample (see Fig. 4B). These iron oxides and hydroxides can react on an acidic and highly sulfated surface, resulting in the corresponding sulfates, which are known to be able to cause serious structural damages over time [32]. This type of reaction is made possible by the high amount of sulfates in solution on the surface of this material [33]. The XRD analysis performed on the same sample does not reveal the presence of (para)coquimbite. Because XRD can only detect compounds whose abundance is higher than the 5% of the total amount of the sample, (para)coquimbite may be a minor/trace component in this sample. On the contrary, compounds such as thenardite, calcite, niter, syngenite, and halite were clearly detected using this technique (see Fig. 3E). The presence of halite (NaCl) and syngenite is closely connected to the influence of marine aerosol [34]. The studied houses are located approximately 2 km from the sea; therefore, the influence of marine aerosol cannot be rejected. To corroborate the XRD data SEM-EDS analyses were also carried out, from which mineralization products containing Ca, C, Na, S, K, and Cl were detected (see Fig. 3C). These results are in accordance with the XRD observations.

House 3

Raman measurements were carried out on the efflorescences from the joint mortars of the bricks used in the construction of House 3. These efflorescences appear as acicular crystals growing from the joint mortar when viewed using a microscope. It is worth noting that the samples were collected from the northwest-facing facade of the house, which experiences the least amount of sunlight.

The Raman spectra revealed the presence of thenardite in the samples studied. In addition to the main band of this sodium sulfate located at 992 cm^{-1}, a small band at 975 cm^{-1} was also identified (see Fig. 5A) as the ν_1 symmetric stretching mode of the SO_4^{2-} group of mascagnite ($(NH_4)_2SO_4$). This mineral is present neither in the original composition of the brick nor in the joint mortar and therefore can be considered a deterioration compound. House 3 has a garden that is connected to the portion of the facade where these efflorescences were identified. This arrangement enables infiltration waters to carry ammonium nitrate (NH_4NO_3) from the decomposition of the plants and green grass of the garden to the facade. The sulfate compounds included intentionally in

the original facade composition can dissolve and react with the ammonium, resulting in the formation of ammonium sulfate. In this reaction, the cation partnered with the sulfate reacts with the nitrate ions carried in the infiltration waters to form the respective nitrate mineralization products. The described reaction pathway can be considered as

$$CaSO_4.2H_2O \rightarrow Ca^{2+} + SO_4^{2-} + 2\ H_2O \quad (2)$$

$$2\ NH_4NO_3 + CaCO_3 \rightarrow Ca(NO_3)_2 + HCO_3^- + NH_3\,(g) + NH_4^+ \quad (3)$$

$$2\ HCO_3^- + FeO \rightarrow FeCO_3 + 2\ H_2O \text{ or mixed carbonate} \quad (4)$$

$$2NH_4^+ + SO_4^{2-} \rightarrow (NH_4)_2SO_4 \quad (5)$$

Considering that for the in situ measurements, information from the joint mortar can also be obtained during the direct measurements of the efflorescences on the joint mortars from the brick, original joint mortar without any visual efflorescence was simultaneously characterized. The main components identified by Raman spectroscopy were calcite, quartz, and carbon, indicating that the joint mortar used is a calcareous mortar. In areas of the joint mortar where efflorescence was visually identified, the typically observed bands of charcoal (C) at 1320 and 1595 cm^{-1}, and of thenardite at 450, 467, 620, 632, 645, 992, 1130, and 1152 cm^{-1} were obtained. Additionally, new bands at 166, 280, 718, and 1090 cm^{-1} were also identified. These bands can be assigned to ankerite ($CaFe(CO_3)_2$), which is a mixed carbonate of calcium and iron (see Fig. 5B). The bands at 166 and 280 cm^{-1} correspond to the ionic translations and librations (restricted rotation) of the CO_3^{2-} group of ankerite, while the bands at 718 cm^{-1} and 1090 cm^{-1} correspond to the ν_4 anti-symmetric bending vibration and the ν_1 symmetric stretching vibration of the same moiety.

The identification of mixed calcium and iron carbonate suggest that the reaction pathway outlined above is taking place in this sample (see reaction 4 in the previous reaction pathway).

An additional analysis on other efflorescence samples taken from the joint mortar (see Fig. 5C) revealed the presence of calcite (153, 280, 711, and 1086 cm^{-1}), epsomite (985 cm^{-1}), charcoal (1320 and 1595 cm^{-1}), and limonite (392 cm^{-1}). In the areas where acicular efflorescence was sampled, thenardite (450, 467, 620, 632, 645, 992, 1101, 1130, and 1152 cm^{-1}), niter (715, 1049, 1344, and 1358 cm^{-1}), nitratine (184, 724, 1067,

and 1385 cm^{-1}) and trona (1062 cm^{-1}) were identified by the Raman spectra, as shown in Fig. 5D.

To confirm the presence of some of these compounds in these efflorescences, XRD and SEM-EDS analyses were also carried out. The XRD analysis of the efflorescences revealed the presence of thenardite, niter, halite, celestite ($Ba_{0.25}Sr_{0.75}SO_4$), and strontium apatite ($Sr_5(PO_4)_3OH$) (see Fig. 3G). These XRD and SEM-EDS results complement those obtained by Raman spectroscopy because these compounds were not detected with the latter technique. It is therefore important to emphasize that the combined used of the three techniques employed is an adequate strategy for extracting the maximum information on the mineralization products present in recently formed efflorescences. The SEM-EDS measurements performed on these efflorescences revealed the presence of S, Na, N, K, and Cl (see Fig. 3F), which confirms the crystallization of thenardite, niter, and halite. The analysis performed via SEM-EDS did not exhibit the presence of Ba, Sr, and P in the efflorescences. However, the fact that in contrast to XRD, SEM-EDS is a microscopic analysis technique must be taken into account. It is likely that celestite and apatite were not present in the selected microscopic areas used in the EDS analysis; therefore, the elements mentioned above were not detected with EDS.

CONCLUSIONS

The principal source of deterioration affecting the building materials present in the modern houses studied in this work is the mineralization of salts. This type of crystallization is primarily external (efflorescence), which affects the integrity and durability of the materials as well as the aesthetic appearance of the facades.

The data obtained from the analyses carried out mainly in situ and in the laboratory, gives an overview of the deterioration products that are present in bricks, artificial stones, and their joint mortars sampled from recently constructed houses.

The Raman spectroscopy, XRD, and SEM-EDS results revealed the presence of thenardite (Na_2SO_4) in most of the efflorescences from all of the houses studied. Mirabilite ($Na_2SO_4 \cdot 10H_2O$) and thenardite (Na_2SO_4) formation on porous building

materials such as mortar is a common pathology cited by many authors [35, 36]. The identification of mirabilite or thenardite by Raman spectroscopy is rather difficult in general because their main spectral bands are quite close (approximately 989 cm^{-1} for mirabilite and approximately 992-993 cm^{-1} for thenardite) [37]. Nevertheless, in this work, well-resolved Raman spectra that also contained medium- and small-intensity bands were obtained, allowing us to affirm that sodium sulfate is mainly crystallized as thenardite. The deterioration process that generates these types of crystallized sulfate salts inside the pores of the material leads to possible cracks and even breaks in the material during the transition from thenardite to mirabilite. The change in the number of waters of hydration during this transition causes increases and/or decreases in the volume of the crystallized sodium sulfates. This change in volume promotes the expansion and contraction of the material in which these salts are crystallized, leading to fissures and cracks.

According to the results presented in this work, we propose that the mortars used in the construction of these houses are composed of a mixture of additives such as K_2O, MgO, Na_2O, SiO_2, MnO_2, CaO, and Fe_2O_x. This conclusion can be explained by considering the original and deterioration products that have been identified. As many authors have noted, the majority of mortars generally contain these types of additives, and the difference between mortars is based on their proportions. For example, the resistance of mortars to deterioration varies according to these proportions; therefore, the proper mixture of the original components and additives must be selected according to the environment in which these building materials are going to be used. Figure 6 displays a schematic representation of the deterioration pathway identified in the analyzed building materials. During the setting of the bricks and mortars, the additives (oxides) included in their composition can be carbonated by atmospheric CO_2, yielding the corresponding carbonates. These carbonates can be subsequently attacked by nitrate salts (typically ammonium nitrate) transported by infiltration waters, causing the formation of new nitrates salts on the surface (efflorescence) or inside the pores of the building material (sub-efflorescence).

In addition to the identified nitrates, various types of sulfate salts were also detected. The joint mortar used in these constructions can contain a high load of sulfates, which can dissolve and subsequently dissociate in solution, facilitating the reaction of these

ions with the cations from the dissociated salts carried in infiltration waters. This process is responsible for the formation of the corresponding sulfates (see Fig. 6). Moreover, the presence of chlorides in the form of halite also suggests the possible influence of marine aerosol on the formation of these recently formed efflorescences. Considering that the homes are in close proximity to the coast (2 km), this hypothesis cannot be rejected.

We have demonstrated that portable in situ Raman spectroscopy is a highly useful technique for the diagnosis of the discussed pathologies in building materials. A subsequent complementary Raman analysis of extracted samples in the laboratory yields the maximum amount of information, which is helpful for predicting the deterioration processes taking place in the considered building materials. Accompanying techniques such as SEM-EDS and XRD have also been proven to be very useful for the identification of compounds such as pyrolusite and anapaite. There have been no literature reports to date that describe deterioration prevention strategies executed on modern building materials, including those used in detached houses intended for use as private homes. Therefore, the discussion contained in this work regarding the original composition of building materials and the newly formed deterioration products will be helpful toward the proposal of prevention strategies that thwart or minimize the deterioration of these materials due to environmental impact.

ACKNOWLEDGEMENTS

This work was financially supported by DEMBUMIES (ref.BIA2011-28148) and funded by the Spanish Ministry of Economy and Competitiveness (MINECO). H. Morillas is grateful to the University of the Basque Country (UPV-EHU) and particularly to the UFI 11-26 Global Change and Heritage, who funded his pre-doctoral fellowship. Technical support provided by the Raman-LASPEA and General X-ray Service: Rocks and Minerals laboratories of SGIker (UPV/EHU, MICINN, GV/EJ, ERDF and ESF) is also gratefully acknowledged.

REFERENCES

[1] F.J. Alejandre, R. Villegas, Mater. Construcc. 59 (2009) 85-103.

[2] L.M. Snell, B.G. Snell, Concrete International 22 (2000) 83-85.

[3] R. Bustamante, J. Monjo, M.I. Sanchez de Rojas, Mater. Construcc. 62 (2012) 309-318.

[4] M. Barsottelli, G.F. Cellai, F. Fratini, C. Manganelli Del Fà, Mater. Struct. 34 (2001) 211-216.

[5] M. Maguregui, A. Sarmiento, I. Martinez-Arkarazo, M. Angulo, K. Castro, G. Arana, N. Etxebarria, J.M. Madariaga, Anal. Bioanal. Chem. 391 (2008) 1361-1370.

[6] F. Fratini, E. Pecchioni, L. Rovero, U. Tonietti, Appl. Clay Sci. 53 (2011) 509-516.

[7] K. Castro, M. Pérez-Alonso, M.D. Rodríguez-Laso, J.M. Madariaga, J. Raman Spectrosc. 35 (2004) 704-709.

[8] J. Ruedrich, M. Seidel, E. Rothert, S. Siegesmund, Building Stone Decay: From Diagnosis to Conservation , E-Publishing Inc., London, 2007, pp. 199-209.

[9] N. Prieto-Taboada, M. Maguregui, I. Martinez-Arkarazo, M.A. Olazabal, G. Arana, J.M. Madariaga, Anal. Bioanal. Chem. 399 (2011) 2949–2959.

[10] D. Kolokotsa, P. Maravelaki-Kalaitzaki, S. Papantoniou, E. Vangeloglou, M. Saliari, T. Karlessi, M. Santamouris, Sol. Energy 86 (2012) 1648-1659.

[11] A. Broggi, E. Petrucci, M.P. Bracciale, M.L. Santarelli, J. Raman Spectrosc. 43 (2012) 1560-1566.

[12] R.N. Yong, V.R. Ouhadi, Appl. Clay Sci. 35 (2007) 238-249.

[13] M. Maguregui, A. Sarmiento, R. Escribano, I. Martinez-Arkarazo, K. Castro, J.M. Madariaga, Anal. Bioanal. Chem. 395 (2009) 2119-2129.

[14] J.I. Alvarez, I. Navarro, A. Martín, P.J. García Casado, Cem. Concr. Res. 30 (2000) 1413–1419.

[15] G. Cultrone, I. Sidraba, E. Sebastián, Appl. Clay Sci. 28 (2005) 297–308.

[16] L. Rampazzi, R. Budini, e-PS, 3 (2006) 21–26.

[17] B. Ipekoglu, H. Böke, O. Cizer, Build. Environ. 42 (2007) 970–978.

[18] M. Perez-Alonso, K.Castro, J.M. Madariaga, Current Anal. Chem. 2 (2006) 89-100.

[19] P. Lopez-Arce, A. Zornoza-Indart, C. Vazquez-Calvo, M. Gomez-Heras, M. Alvarez de Buergo, R. Fort, Spectrosc. Lett. 44 (2011) 505-510.

[20] H. Morillas, M. Maguregui, O. Gómez-Laserna, J. Trebolazabala, J.M. Madariaga, J. Raman Spectrosc. 43 (2012) 1630–1636.

[21] M. Maguregui, N. Prieto-Taboada, J. Trebolazabala, N. Goienaga, N. Arrieta, J.Aramendia, L. Gomez-Nubla, A. Sarmiento, M. Olivares, J.A. Carrero, I. Martinez-Arkarazo, K. Castro, G. Arana, M.A. Olazabal, L.A. Fernandez, J.M. Madariaga. CHEMCH 1st International Congress Chemistry for Cultural Heritage, Ravenna, 30th June–3rd July, 2010.

[22] R.T. Downs, M. Hall-Wallace, A Database of Crystal Structures Published in the American Mineralogist and The Canadian Mineralogist and Its Use as a Resource in the Classroom. 18th General Meeting of the International Mineralogical Association (2002) page 128.

[23] H. Morillas, M. Maguregui, O. Gómez-Laserna, J. Trebolazabala, J.M. Madariaga, J. Raman Spectrosc. 44 (2013) 1700–1710.

[24] M. Maguregui, U. Knuutinen, K. Castro, J.M. Madariaga, J. Raman Spectrosc. 41 (2010) 1400-1409.

[25] A. Sarmiento, M. Maguregui, I. Martinez-Arkarazo, M. Angulo, K. Castro, M.A. Olazábal, L.A. Fernández, M.D. Rodríguez-Laso, A. M. Mujika, J. Gómez, J.M. Madariaga, J. Raman Spectrosc. 39 (2008) 1042-1049.

[26] F. Veniale, M. Setti, C. Rodriguez-Navarro, S. Lodola, W. Palestra, A. Busetto, Cement & Concrete Composites 25 (2003) 1123-1129.

[27] V. S. Ramachandran, J. J. Beaudoin. Handbook of Analytical Techniques in Concrete Science and Technology. Principles, Techniques and Applications. William Andrew Publishing, New York, 2001.

[28] B.E.I. Abdelrazig, J.H. Sharp, B.El-Jazairi, Cem. Concr. Res. 18 (1988) 415-25.

[29] N.E. Hipedinger, A.N. Scian, E.F. Aglietti, Cem. Concr. Res. 32 (2002) 675-682.

[30] C. Julien, M. Massot, R. Baddour-Hadjean, S. Franger, S. Bach, J.P. Pereira-Ramos, Solid State Ionics 159 (2003) 345–356.

[31] M. Maguregui, U. Knuutinen, I. Martinez-Arkarazo, K. Castro, J.M. Madariaga, Anal. Chem. 83 (2011) 3319-3326.

[32] S.S. Potgieter-Vermaak, J.H. Potgieter, R. Van Grieken, Cem. Concr. Res. 36 (2006) 656 – 662.

[33] A. El-Turki, R.J. Ball, G.C. Allen, Cem. Concr. Res. 37 (2007) 1233–1240.

[34] P.Vargas Jentzsch, B. Kampe,V. Ciobotă, P. Rösch, J. Popp, Spectrochim. Acta A 115 (2013) 697-708.

[35] M. Steiger, S. Asmussen, Geochim. Cosmochim. Ac. 72 (17) (2008) 4291-4306.

[36] C. Rodriguez-Navarro, E. Doehne, E. Sebastian, Cem. Concr. Res. 30 (2000) 1527-1534.

[37] A. Hamilton, R.I. Menzies, Raman spectra of mirabilite, J. Raman Spectrosc. 41 (2009) 1014-1020.

FIGURE CAPTIONS

Fig. 1. (A) Location and details of the analyzed areas containing the detached houses (Metropolitan Bilbao, North of Spain). **(B)** Schematic representation of the pathologies identified in the three detached houses considered in this work.

Fig. 2. (A) Raman spectrum of efforescences in bricks indicating the presence of epsomite ($MgSO_4 \cdot 7H_2O$) and niter (KNO_3). **(B)** Raman spectrum of mortar showing bands of thenardite (Na_2SO_4), niter (KNO_3), and nitratine ($NaNO_3$). **(C)** Raman spectrum of efflorescences in mortar showing bands of thenardite (Na_2SO_4), niter (KNO_3), trona ($Na_3(HCO_3)(CO_3) \cdot 2H_2O$), calcite ($CaCO_3$), and dolomite ($MgCaCO_3$). **(D)** Raman spectrum of joint mortar showing the bands of quartz (SiO_2), pyrolusite (MnO_2), and anapaite ($Ca_2Fe^{2+}(PO_4)_2 \cdot 4\ H_2O$).

Fig. 3. (A) SEM-EDS results of joint mortar from House 1 showing pyrolusite and anapaite. **(B)** XRD diagram of joint mortars from House 1 showing calcite, anapaite, quartz and pyrolusite. **(C)** SEM-EDS of efflorescences from House 2 showing calcite, thenardite, syngenite, and halite. **(D)** XRD diagram of whitish patinas from House 2 showing calcite, anapaite, quartz, and pyrolusite. **(E)** XRD diagram of another patina from House 2 showing thenardite, calcite, niter, syngenite, and halite. **(F)** SEM-EDS of whitish patina from House 3 showing thenardite, niter, and halite. **(G)** XRD diagram of whitish patina from House 3 showing thenardite, niter, halite, celestite, and strontium apatite.

Fig. 4. (A) Raman spectrum of whitish patina on artificial stone showing bands of manganese oxide (MnO), syngenite ($K_2Ca(SO_4) \cdot H_2O$), gypsum ($CaSO_4 \cdot 2H_2O$), (para)coquimbite ($Fe_2(SO_4)_3 \cdot 9H_2O$) and calcite ($CaCO_3$). **(B)** *Measurement 1*: Raman spectrum of the same sample of artificial stone, showing bands belonging to limonite ($Fe_2O_4 \cdot H_2O$) and calcite ($CaCO_3$). *Measurement 2*: Raman spectrum of artificial stone showing bands of hematite (Fe_2O_3).

Fig. 5. (A) Raman spectrum of efflorescences on bricks showing bands of thenardite (Na_2SO_4) and a band at 975 cm^{-1} assigned to mascagnite ($(NH_4)_2SO_4$). **(B)** Raman spectrum of mortars showing bands of thenardite (Na_2SO_4), charcoal (C) and ankerite ($CaFe(CO_3)_2$). **(C)** Raman spectrum of calcite ($CaCO_3$), epsomite ($MgSO_4 \cdot 7\ H_2O$),

charcoal (C), and limonite ($Fe_2O_4 \cdot H_2O$). **(D)** Raman spectrum of efflorescence showing bands of thenardite (Na_2SO_4[1]), niter (KNO_3), nitratine ($NaNO_3$), and trona (($Na_3(HCO_3)(CO_3) \cdot 2H_2O$).

Fig. 6. Schematic representation of the deterioration pathway described in the text for the analyzed bricks, joint mortars, and artificial stones.

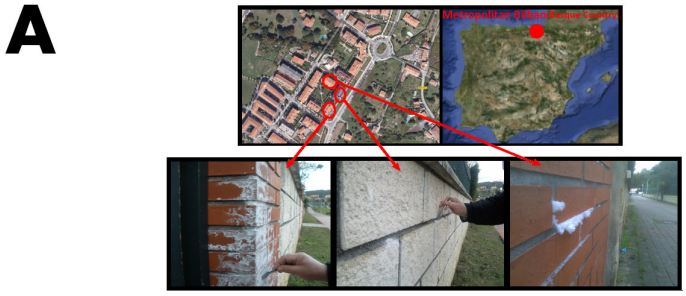

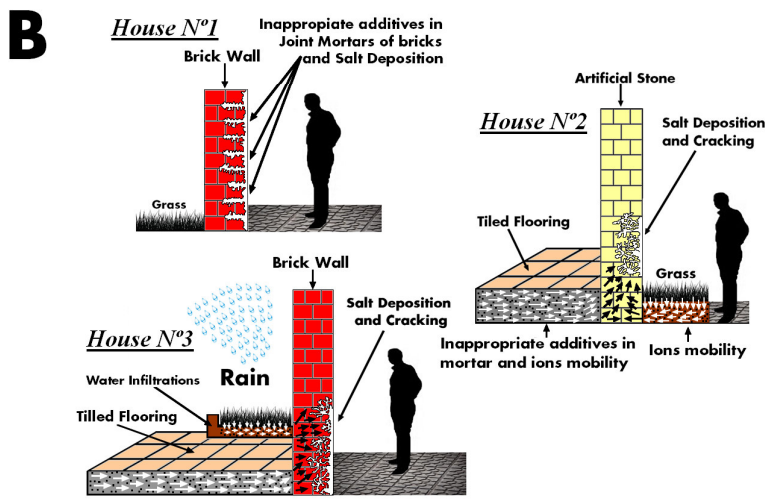

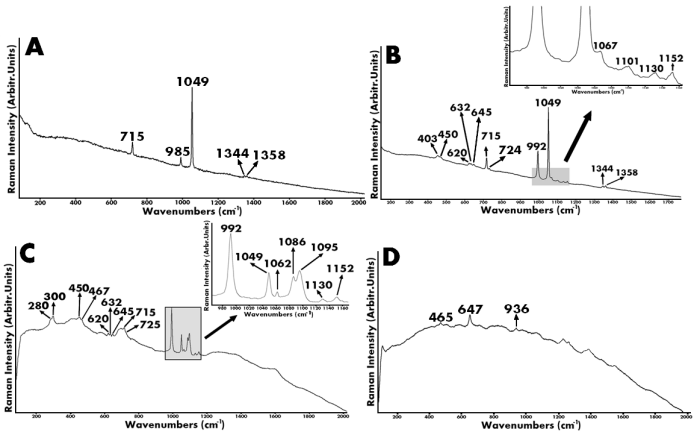

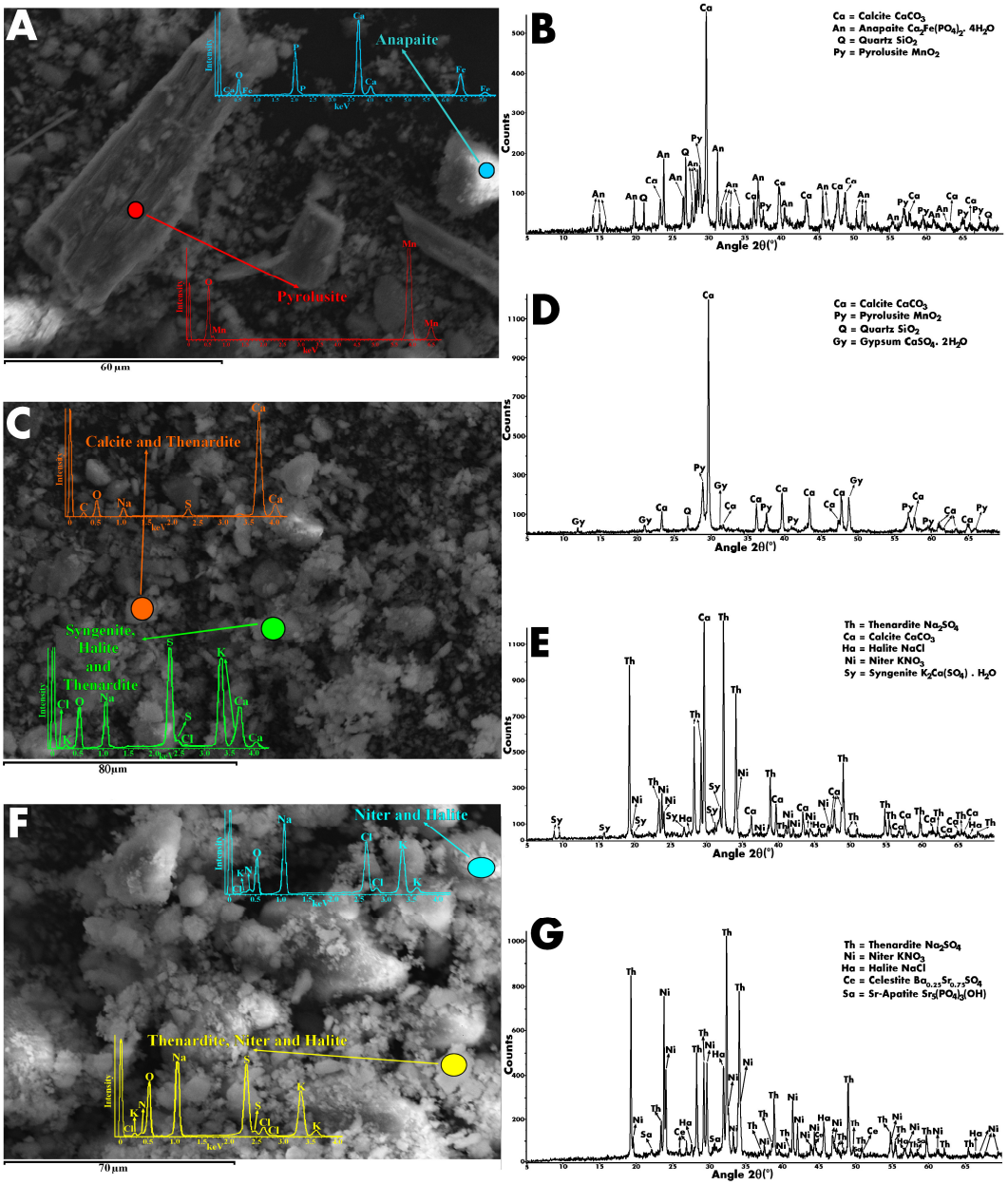

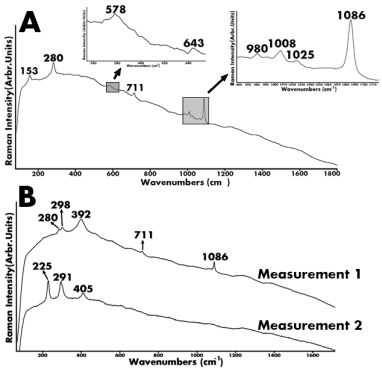

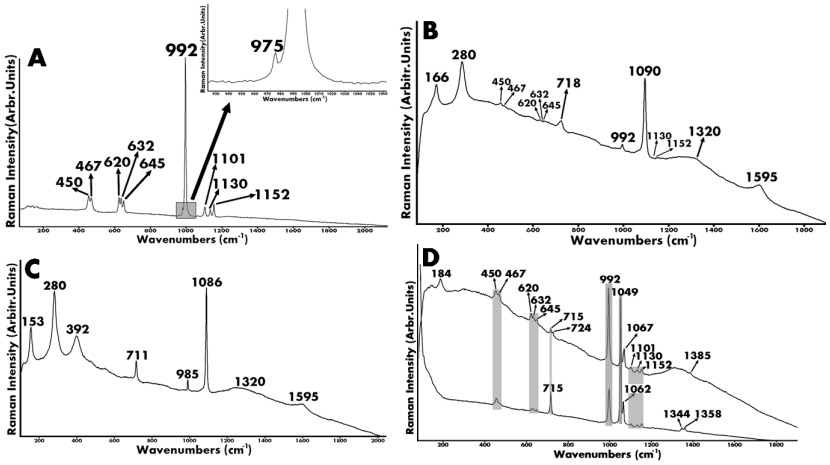

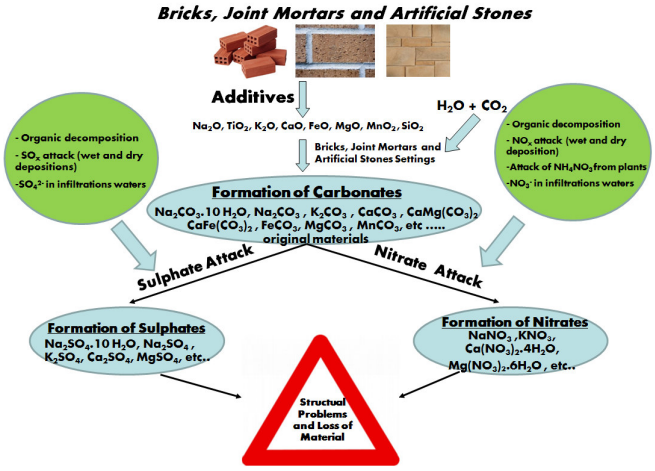

HIGHLIGHTS

- Building materials of recently erected houses were characterized by Raman spectroscopy, SEM-EDS and XRD.
- In situ analysis with portable instrumentation was useful to evaluate their conservation state.
- Bricks, joint mortars and artificial stones were highly affected by sulphation processes.
- Ammonium nitrate was the responsible of the nitrate salts crystallizations.
- The integration of appropriate additives in building materials is essential for their preservation.